


## RESEARCH ARTICLE

# PCL-*b*-PnBA Additives Enable Flexible and Adhesive Photoresists through Microphase Separation

Shibiru Yadeta Ejeta<sup>1</sup> | Trupti Bambalkar<sup>1</sup> | Shiao-Wei Kuo<sup>2</sup> | Mao-Feng Hsu<sup>3</sup> | Hsin-Min Wang<sup>1</sup> | Kuan-Yu Kuo<sup>1</sup> | Chih-Feng Huang<sup>1,4</sup> 

<sup>1</sup>Department of Chemical Engineering, i-Center For Advanced Science and Technology (iCAST), National Chung Hsing University, Taichung 40227, Taiwan |

<sup>2</sup>Department of Materials and Optoelectronic Science, Center for Functional Polymers and Supramolecular Materials, National Sun Yat-Sen University, Kaohsiung 80424, Taiwan | <sup>3</sup>Zhen Ding Technology Holding Limited, Taoyuan 33754, Taiwan | <sup>4</sup>Graduate Program in Semiconductor and Green Technology, Academy of Circular Economy, National Chung Hsing University, Nantou County 540216, Taiwan

**Correspondence:** Mao-Feng Hsu ([brian.mf.hsu@zdtco.com](mailto:brian.mf.hsu@zdtco.com)) | Chih-Feng Huang ([huangcf@dragon.nchu.edu.tw](mailto:huangcf@dragon.nchu.edu.tw))

**Received:** 7 September 2025 | **Revised:** 19 October 2025 | **Accepted:** 31 October 2025

**Keywords:** additives | block copolymers | PCL-*b*-PnBA | photoresists | ROP | SARA ATRP

## ABSTRACT

Photoresists (PRs) are light-sensitive polymers used in photolithography to fabricate micropatterns on substrates. This study proposes a microphase separation strategy to overcome the flexibility limitations associated with typical acrylic-based PRs in patterning applications by incorporating poly( $\epsilon$ -caprolactone)-*b*-poly(*n*-butyl acrylate) (PCL-*b*-PnBA) block copolymer (BCP) additives. A BCP additive was prepared using a dual-functional initiator, ethyl 2-hydroxyethyl-2-bromoisobutyrate (HEBiB), which can efficiently combine two eco-friendly polymerization techniques of ring-opening polymerization (ROP) and supplemental activator and reducing agent atom transfer radical polymerization (SARA ATRP) (i.e., ROP-*C*-SARA ATRP), allowing for precise control over compositions and compatibility. For synthesizing the PRs, methyl methacrylate (MMA), acrylic acid (AA), and maleic anhydride (MAN) monomers were utilized to afford two randomly copolymerized pre-polymers, namely, P(MMA-*r*-AA) and P(MMA-*r*-MAN). Following esterification with allyl bromide and hydroxyethyl methacrylate (HEMA), two PR systems (abbreviated as PMAV and PMMANMA, respectively) were prepared. By mixing various amounts of the PCL<sub>119</sub>-*b*-PnBA<sub>96</sub> ( $M_{n,NMR}$  = 26,080;  $\Phi_{PCL}$  = 0.49;  $D$  = 1.28) and two PRs following UV-curing reactions, high transmission films can be obtained. Their photopatterning and mechanical properties were improved, owing to the occurrence of microphase separation within the matrix. Microstructure-containing matrices were characterized by small-angle X-ray scattering (SAXS). The compatibility of the BCP additive with commercially available polyimide acrylate (PIA) and polyurethane acrylate (PUA) PRs was examined. Lithographic evaluations showed improved resolution, uniformity, and developer resistance, highlighting the potential of PCL-*b*-PnBA-modified resins for high-performance photoresists in flexible electronic fabrications and next-generation lithography.

## 1 | Introduction

Photoresists (PRs) are photosensitive materials that are used in photolithography and photoengraving to create patterned surface coatings [1]. They are essential in micro- or nanofabrication

technologies, especially in the production of semiconductors, printed circuit boards, and photosensitive insulating layers, as ink coatings for flexible circuit boards, and more recently in biomedical and optical applications [2]. The main matrix ensures strong substrate adhesion and provides suitable mechanical

Shibiru Yadeta Ejeta and Trupti Bambalkar contributed equally to this work as the first authors.

properties [3, 4]. In contrast, additives are essential for enhancing specific characteristics for photolithography [5, 6]. For overall formulations, key components of the PR matrix, photoinitiators, additives, and solvents serve distinct functions and should be circumspectly considered [7–10].

Regarding the polymer matrix for PRs, photosensitive resins of acrylic, epoxy (EP), polyimide (PI), and polyurethane (PU) with distinct chemical structures and properties have been reported for various valuable applications [11, 12]. Acrylic resins, which are derived from monomers such as acrylic acid (AA), methyl methacrylate (MMA), and hydroxyethyl methacrylate (HEMA), are the most utilized in advanced photoresist materials due to their specific advantages [13, 14]. Likewise, photosensitive EP resins are renowned for their high mechanical strength, chemical resistance, excellent adhesion to various substrates, and good dimensional stability [15]. However, without modifiers, they are relatively brittle and exhibit slow curing times unless catalyzed [16–18]. Polyurethane acrylate (PUA) resins offer high flexibility, abrasion resistance, impact strength, and tunable softness or hardness, along with good elastic recovery [19, 20]. When two or more such resins are mixed, they complement each other, resulting in customized materials with balanced performance, overcoming individual limitations, and enhanced multifunctionality [21]. For example, for flexible circuit boards, photosensitive resin blends comprise acrylic and epoxy resins, which are UV-crosslinked. Such hybrid resins demonstrate a synergistic balance of flexibility and durability achievements [21–25]. In addition, elastic materials are commonly added to improve their softness and flexibility [26]. However, this approach still faces challenges due to poor compatibility between elastomers and polar resins [27, 28]. Additionally, removal of high molecular weight elastomers during the development process is difficult, negatively affecting the imaging quality of the photosensitive resins [29–32].

In addition to the aforementioned compositions, additives also play a crucial role in photosensitive resin compositions by enhancing properties such as flexibility, adhesion, and chemical resistance [33, 34]. Additives serve several important functions, such as increasing light sensitivity [5], enhancing resolution [11], controlling film thickness and adhesion [35], reducing defects [36], and modifying the mechanical and chemical properties of the resist [37]. Therefore, the efficiency and reliability of photolithographic processes in semiconductor manufacturing, microfabrication, and related applications can be significantly enhanced by carefully selecting appropriate additives.

Several strategies have been demonstrated for preparing diverse functional copolymers, including chain-end transformations or post-modifications coupled with subsequent reactions, the use of dual-functional initiators or inimers in multistep or one-step polymerizations, and grafting methods for nonlinear copolymers. These approaches provide versatile pathways to tailor architectures such as star copolymers and bottlebrush polymers, while requiring careful consideration of site reactivity and compatibility between different polymerization techniques. Various combination approaches—denoted by the symbol “C”—used in diverse and robust polymerization systems have been reported. Several studies have highlighted the integration of controlled/living polymerization (CLP) techniques with efficient

chemical reactions to develop novel polymeric materials and explore their distinctive properties and potential applications [38–42]. Through synergy with “green” polymerization methods, this synthetic strategy enables sequential polymerization to yield well-defined copolymers that integrate both degradable and functional segments. For example, ring-opening polymerization (ROP) can be achieved via an eco-friendly organo-catalyst and followed by supplemental activator and reducing agent atom transfer radical polymerization (SARA ATRP) via a ppm level of catalyst (i.e., ROP-C-SARA ATRP) [43], as well as the reverse process is also possible [44]. Thus, using a dual-functional initiator is a promising and effective strategy to produce tailor-made block copolymers (BCPs) [45–47].

To attain high performance, the development process of PR features is also important. Reaction-induced microphase separation (RIMPS) [48, 49] or a similar approach called polymerization-induced microphase separation (PIMS) [50] is a highly effective technique for constructing micro- and nanoscale structures within polymeric matrices. When a BCP with compatible and incompatible blocks is applied, microstructures are formed within the polymeric matrix through RIMPS or self-assembly (SA) mechanisms [51]. For example, Boyer demonstrated a method that combined photopolymerization with in situ microphase formation to construct highly ordered morphologies [50, 52]. Thus, RIMPS or PIMS can simultaneously fabricate ordered morphology, streamline processing by reducing steps, and offer enhanced tunability along with improved mechanical stability and pattern fidelity [52]. Its tunability with a wide range of materials, along with the potential for solvent-free or aqueous processing [52, 53], makes RIMPS an attractive option for environmentally friendly and multifunctional applications.

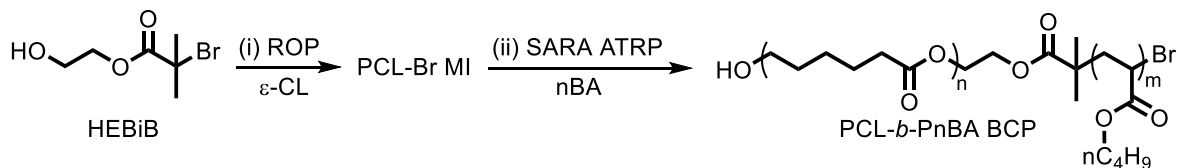
This study investigates photosensitive resins incorporating the block copolymer additive poly( $\epsilon$ -caprolactone)-*b*-poly(*n*-butyl acrylate) (PCL-*b*-PnBA), in which the compatible PCL block [54] and the incompatible PnBA block render microphase during crosslinking [55]. A dual-functional initiator bearing both hydroxyl (for ROP) and halo-ester (for SARA ATRP) groups was prepared to enable a sequential polymerization approach. The resulting PCL-*b*-PnBA additive enhances film formation, mechanical strength, and substrate adhesion, making it suitable for flexible photoresist and ink coatings. In particular, PnBA exhibits elastomeric properties due to its low glass transition temperature ( $T_g = -53^\circ\text{C}$ ) and also offers facile degradation under UV irradiation. Various acrylic acid-based resins blended with PCL-*b*-PnBA were prepared, characterized, and evaluated. The materials exhibited high flexibility, resolution, and etch resistance, indicating their potential for industrial photoresist applications.

## 2 | Experimental Section

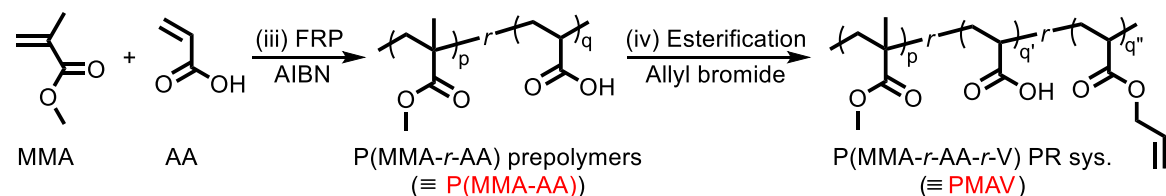
### 2.1 | Materials

Methyl methacrylate (MMA, 99%), acrylic acid (AA, 97%), hydroxyethyl methacrylate (HEMA, 98%), propylene glycol monomethyl ether acetate (PGMEA, 97%), and *n*-butyl acrylate (nBA, 99%) were purchased from Sigma-Aldrich Co. Allyl bromide (98%),  $\epsilon$ -caprolactone ( $\epsilon$ -CL, 98%),  $\text{K}_2\text{CO}_3$  (99%), ethyl glycol

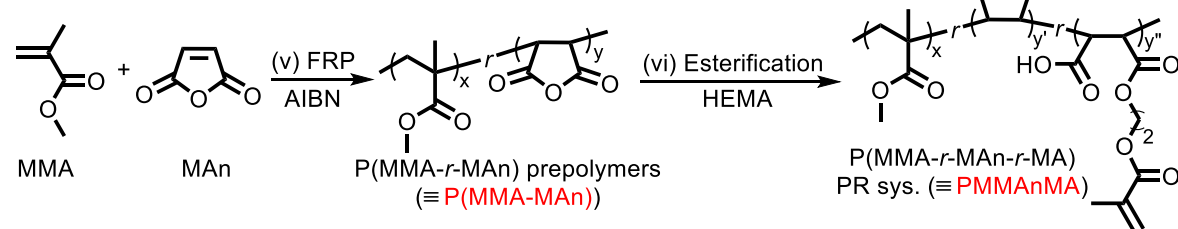
(a) Synthesis of block copolymer (BCP) via a ROP- $\epsilon$ -SARA ATRP approach:



(b) Synthesis of photoresist with pendant vinyl group (i.e., PMAV system):



(c) Synthesis of photoresist with pendant methacrylic group (i.e., PMMAAnMA system):



**SCHEME 1** | Synthetic routes for (a) PCL-*b*-PnBA BCP via a ROP- $\epsilon$ -SARA ATRP approach, (b) PMAV PR system via MMA/AA FRP followed by allyl bromide post-esterification, and (c) PMMAAnMA PR system via MMA/MAn FRP followed by HEMA post-esterification.

(EG, 99%), diphenyl phosphate (DPP, 98%), 2-bromoisobutyryl bromide (BiB, 98%), copper bromide (CuBr, 97%), copper wire (Cu(0)), pentamethyl diethylenetriamine (PMDETA, 99%), maleic anhydride (MAn, 97%), and 2,2-azobis(isobutyronitrile) (AIBN, 99%) were purchased from Acros chemicals. Isopropylthioxanthone (ITX, 99%), Irgacure 907 (98%), epoxy acrylate (EPA, MW = 13,000; acid value (AV) = 97.3 eq/g), polyimide acrylate (PIA, MW = 10,000; AV = 57.8 eq/g), and polyurethane acrylate (PUA, MW = 19,500; AV = 104.3 eq/g), were supported from Zhen Ding Technology Holding Limited. The synthesis of ethyl 2-hydroxyethyl-2-bromoisobutyrate (HEBiB) dual-functional initiator is referred to the previous literature [49].

## 2.2 | Synthesis Methods

### 2.2.1 | Synthesis of PCL-*b*-PnBA Additives via the ROP- $\epsilon$ -SARA ATRP Approach [42, 48]

As shown in Scheme 1a, the synthesized HEBiB initiator (see Scheme S1) was subjected to ROP of  $\epsilon$ -CL to produce PCL-Br macroinitiator (MI) for the next SARA ATRP. HEBiB,  $\epsilon$ -CL, and DPP were mixed with toluene ( $\epsilon$ -CL/HEBiB/DPP = 160:1:1; [ $\epsilon$ -CL]<sub>0</sub> = 4.5 M) in a Schlenk bottle and placed in an oil bath at 40°C. After the reaction was completed, the mixture was diluted with THF and reprecipitated with methanol. The solid was collected and dried; thus, a white powder of PCL<sub>119</sub>-Br MI ( $M_{n,NMR}$  = 13,800;  $D$  = 1.08; yield = 80%) was obtained.

As shown in Scheme 1a, a combination ( $\epsilon$ ) approach of ROP- $\epsilon$ -SARA ATRP was then conducted through the chain extension of PCL-Br with nBA and catalyzed by CuBr, Cu(0), and PMDETA. A mixture with a molar ratio of nBA/PCL-

Br/CuBr/Cu(0)/PMDETA = 500:1:0.07:0.14:0.2 was added to a Schlenk flask with anisole as the solvent ([nBA]<sub>0</sub> = 1.8 M). A freeze-thaw pump circulation method was employed to remove oxygen. The flask was then placed in an oil bath at 100°C. After the reaction was complete, the Schlenk flask was cooled in an ice bath and exposed to air to stop the polymerization. The resulting product was diluted with THF and reprecipitated using ice-cold methanol. The yellowish white powder was collected, and any residual solvent was removed in a vacuum oven to afford the additive of PCL<sub>119</sub>-*b*-PnBA<sub>96</sub> BCP ( $M_{n,NMR}$  = 26,080;  $D$  = 1.28;  $\Phi_{PCL}$  = 0.49; yield = 40%).

### 2.2.2 | Synthesis of Two Photoresist (PR) Systems

As shown in Scheme 1b,c, two PR systems were designed. Step (iii) for FRP of MMA and AA using AIBN was first conducted to synthesize the abbreviated PMAV system as shown in Scheme 1b (MMA/AA/AIBN = 30:210:*x* in DMF (*x* = 5 or 10); [MMA]<sub>0</sub> = 1.9 M). After the reaction was completed, the mixture was concentrated and reprecipitated with ethyl acetate to afford P(MMA-*r*-AA) prepolymers (*r*: random; denoted as P(MMA-AA)). Subsequently, the resulting prepolymers were modified with allyl bromide (step (iv) in Scheme 1b) and K<sub>2</sub>CO<sub>3</sub> in DMAc at room temperature to afford the P(MMA-*r*-AA-*r*-V) PR system (abbreviated as PMAV). The modified molar percentages (i.e.,  $q''/q \times 100\%$ ) were approximately 50%. To synthesize the abbreviated PMMAAnMA system shown in Scheme 1c, step (v) for FRP of MMA and MAn using AIBN was thus conducted (MMA/MAn/AIBN = 30:210:*x* (*x* = 10 or 15) in THF at 65°C; ([MMA]<sub>0</sub> = 1.1 M). The obtained prepolymers (denoted as P(MMA-MAn)) were subsequently modified with HEMA and pyridine in PGMEA at 100°C (step (vi) in Scheme 1c). After

the reaction was completed, the crude was concentrated and reprecipitated with diethyl ether to afford the P(MMA-*r*-MAN-*r*-MA) PR system (abbreviated as PMMANMA). The modified molar percentages (i.e.,  $y''/y \times 100\%$ ) were approximately 70% and 20%.

## 2.3 | Characterization

The number average molecular weight ( $M_n$ ) and dispersity index ( $\bar{D}$ ) were measured by means of gel permeation chromatography (GPC) using a Malvern OMNISEC system equipped with a RI detector and polystyrene mixed gel columns at 40°C using THF as an eluent and calibrated with PMMA standards. Infrared (IR) spectra were recorded on JASCO FT/IR-6100 with an ATR attachment. The proton nuclear magnetic resonance ( $^1\text{H}$  NMR) spectra of the samples were measured using a 400 MHz JEOL ECS-400 in  $\text{CDCl}_3$  and recorded in ppm ( $\delta$ ). UV-vis absorption spectra were measured using a Jasco V-560 spectrometer. The sample morphologies were observed using a Field Emission SEM (JEOL JSM 7401F, Japan). Small-angle X-ray scattering (SAXS) measurements were conducted at the BL23A1 beamline of the National Synchrotron Radiation Research Center (NSRRC), Taiwan. The X-ray source operated at an energy of 15 kV, with a sample-to-detector distance of 3 m. The d-spacing values were determined from the primary scattering peak positions ( $q^*$ ) using the equation  $d = 2\pi/q^*$ .

## 2.4 | Testing Methods

For the development process study, various PR compositions were composed and coated on copper foils. Then, a baking process at 85°C for 2 h was conducted to prepare the PR dry films. The samples were then exposed to 600 mJ/cm<sup>2</sup> based on reactivity and developed in a 1 wt%  $\text{K}_2\text{CO}_3(\text{aq})$  solution or methanol. Then, the post-baking temperature was set at 150°C for 1 h. The dry films with a thickness of  $100 \pm 10 \mu\text{m}$  were then tested for various physical properties. The acid value (AV (eq/g)) of the prepolymers and PRs was estimated by the titration method with a given mass (W) of the sample and 0.1 N  $\text{KOH}(\text{aq})$  using the equation, acid value (AV) =  $V \times N \times 56.1/W$ , where V is the volume of  $\text{KOH}(\text{aq})$  used in titration (mL), N is the molarity of  $\text{KOH}(\text{aq})$  solution (mol/L), 56.1 is the molecular weight of KOH (g/mol), and W is the weight of the polymer sample (g) [56]. The adhesion strength was examined by a typical cross-cut 100-grid/ASTM D3359 test to conduct a fast screening process. Dead-fold testing was performed by mechanically folding the prepared photoresist material on the substrate for several cycles. For comparison, the resolution and compatibility of the additive were further blended into commercial photosensitive resins, including epoxy acrylate (EPA), polyurethane acrylate (PUA), and polyimide acrylate (PIA) PRs.

## 3 | Results and Discussion

### 3.1 | Synthesis and Characterization of the PCL-*b*-PnBA Additives and Two PR Systems

As shown in Scheme 1a, the additive was synthesized via an efficient and eco-friendly method of ROP- $\epsilon$ -SARA ATRP combination using a dual-functional initiator, HEBiB (the synthetic

route is shown in Scheme S1). As shown in Figure S1A, structural assignments can be clearly revealed by  $^1\text{H}$  NMR, indicating the successful synthesis of high-purity HEBiB. Initiating from the hydroxyl group of HEBiB for ROP of  $\epsilon$ -CL, the kinetic trace was shown in Figure S2a (see the SI:  $\epsilon$ -CL/HEBiB/DPP = 160:1:1;  $[\epsilon\text{-CL}]_0 = 4.5 \text{ M}$  in toluene at 40°C). The apparent reaction rate constant ( $k_{\text{app}(\epsilon\text{-CL})}$ ) was calculated to be  $4.28 \times 10^{-5} \text{ s}^{-1}$ , as determined by linear regression analysis of the natural logarithmic plots of reactant concentration changes versus time (i.e.,  $\text{Ln}(M_0/M)$  vs.  $t$ ) that showed a first-order reaction. As shown in Figure S2b, the GPC trace of the resultant demonstrated a monodisperse with low  $\bar{D}$  value ( $M_{n,\text{GPC}} = 16,000$ ;  $\bar{D} = 1.08$ ). These results indicate a typical controlled/living polymerization (CLP) fashion. The resultant was also analyzed by  $^1\text{H}$  NMR, as shown in Figure 1A. Major signals of peaks a–d from the PCL backbone were observed. Notably, the isobutyryl bromoester end can also be observed (i.e., peak e), which can be further estimated the molecular weight ( $M_{n,\text{NMR}} = 13,780$ ). For the subsequent SARA ATRP chain extension of PCL-Br with nBA (nBA/PCL-Br/CuBr/Cu(0)/PMDETA = 500:1:0.07:0.14:0.2 at 100°C;  $[\text{nBA}]_0 = 1.8 \text{ M}$ ), an induction period (ca. 1.5 h) was acquired (shown in Figure S2c). This is plausibly due to the establishment of a dynamic equilibrium concentration between  $\text{Cu}^{\text{I}}$  and  $\text{Cu}^{\text{II}}$  species [57, 58]. After the induction period, a linear regression curve corresponding to a first-order reaction can be obtained with a  $k_{\text{app}(\text{nBA})}$  value of  $3.39 \times 10^{-5} \text{ s}^{-1}$ . As shown in Figure S2d, the GPC trace of the various resultants demonstrated a gradual molecular weight evolution in monomodal and low  $\bar{D}$ . Final product with  $M_{n,\text{GPC}} = 24,330$  and  $\bar{D} = 1.28$  was obtained. As shown in Figure 1B, the  $^1\text{H}$  NMR spectrum displays the original signals from the PCL block (i.e., peaks a'–d') and new signals from the PnBA block (i.e., peaks f–k). Thus, we demonstrated that two eco-friendly polymerization techniques (i.e., ROP- $\epsilon$ -SARA ATRP) can be efficiently combined to synthesize well-defined PCL-*b*-PnBA BCPs. The synthetic conditions and characterization of PCL-Br and PCL-*b*-PnBA are summarized in Table S1.

As illustrated in Scheme 1b, the synthetic step (iii) involved the FRP of MMA and AA in the presence of AIBN as the radical initiator. Polymerization was performed in DMF solvent using a molar feed ratio of MMA/AA/AIBN = 30:210: $x$  ( $x = 5$  or 10;  $[\text{MMA}]_0 = 1.9 \text{ M}$ ). This polymerization step resulted in the formation of an acrylic acid-rich prepolymer, which we designated as P(MMA-AA). The degree of acid functionality in these prepolymers was quantitatively assessed via titration, yielding AVs of approximately 320 and 350 eq/g, depending on the AIBN content. As depicted in step (iv) of Scheme 1b, the P(MMA-AA) was then subjected to post-esterification with allyl bromide (AB), affording the alkene-functionalized polymer system abbreviated as PMAV PR. This structural modification enabled the introduction of pendant vinyl groups, which facilitated subsequent photochemical crosslinking reactions. As shown in Figure 2Ai,Aii for an exemplified comparison, the corresponding IR spectra of P(MMA-AA)I and PMAV1 showed similar signals with a main carbonyl peak (ca. 1730  $\text{cm}^{-1}$ ). As shown in Figure 2Bi,Bii for  $^1\text{H}$  NMR spectra, obvious broad signals of peaks a'–c' (ca. 4.5–6 ppm) from the pendant double bond group were observed, indicating an efficient post-esterification reaction.

As shown in Scheme 1c, step (v) for FRP of MMA and MAN using AIBN was also conducted (MMA/MAN/AIBN = 30:210: $x$



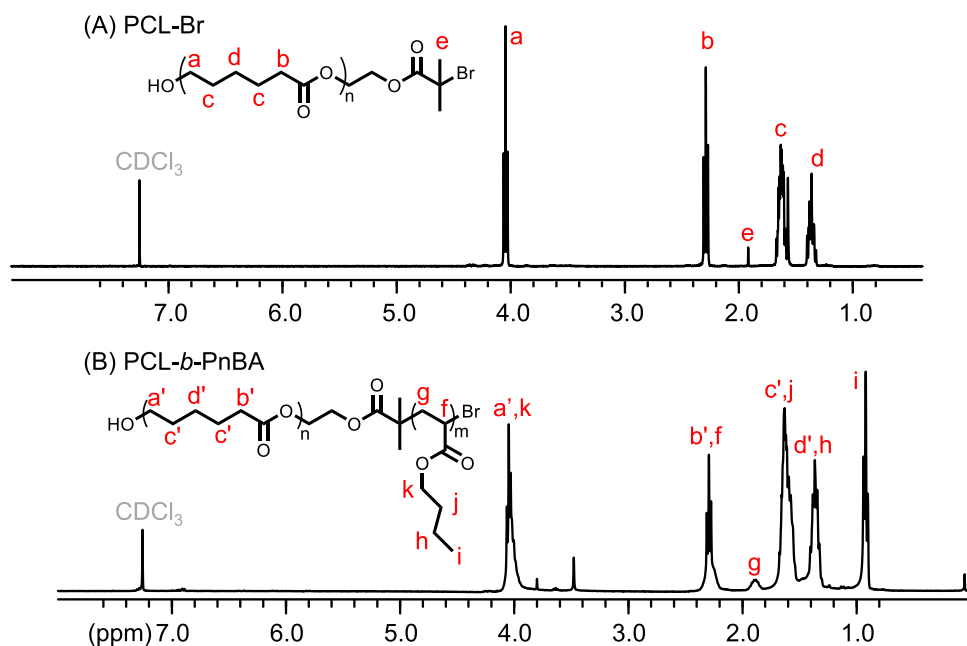


**FIGURE 1** |  $^1\text{H}$  NMR (400 MHz,  $\text{CDCl}_3$ ) of (A) PCL-Br MI and (B) PCL-*b*-PnBA BCP.

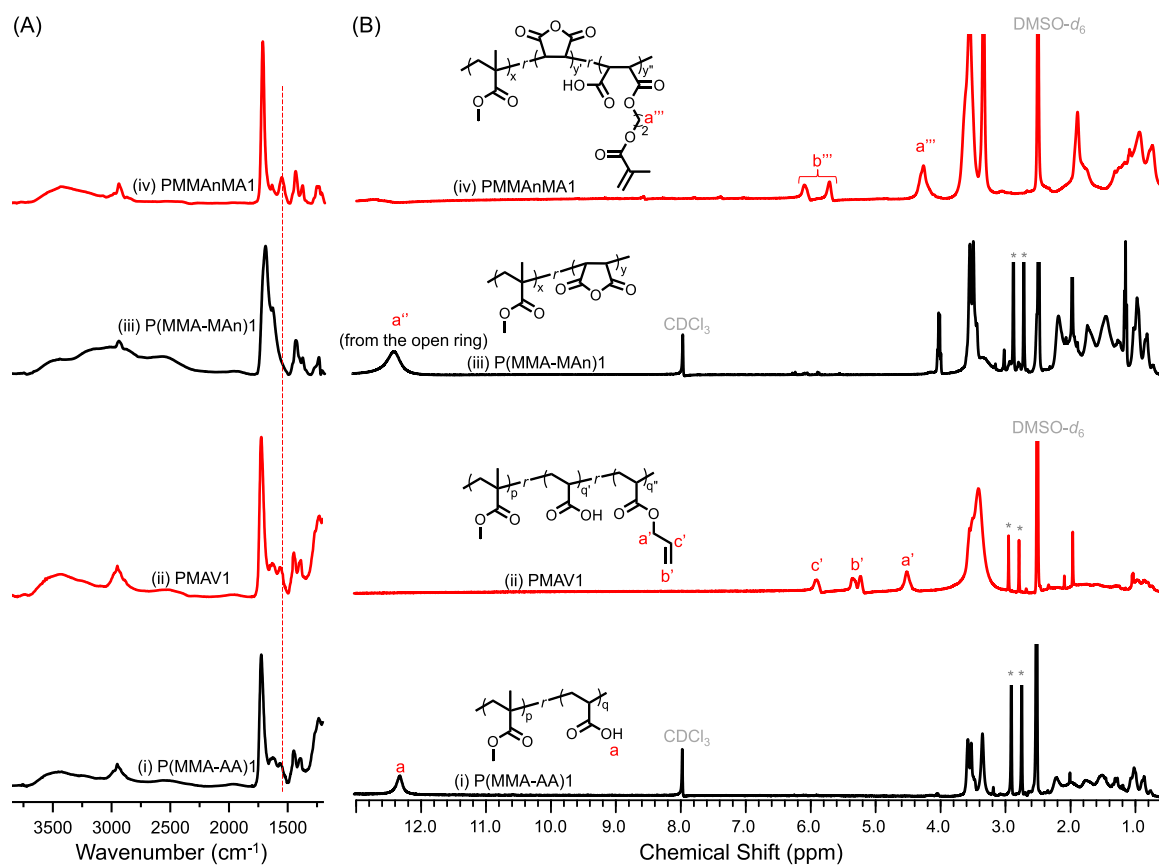


**FIGURE 2** | (A) FTIR spectra and (B)  $^1\text{H}$  NMR (400 MHz) of (i) P(MMA-AA)1 prepolymer, (ii) PMAV1 PR, (iii) P(MMA-MAN)1 prepolymer, and (iv) PMMANMA1 PR.

**TABLE 1** | Reaction compositions and characterization of the two PR systems.

Sample name	Feeding ratio	$M_n$ (Đ) <sup>c</sup>	AV <sup>d</sup> [eq/g]	Esterification agent	Fraction of post-esterification
P(MMA-AA)1	MMA/AA/AIBN <sup>a</sup> = 90/210/5 (by mol.)	17,520 (1.89)	320	—	—
PMVA1	P(MMA-AA)1/AB <sup>b</sup> = 3/1 (by wt.)	20,610 (2.23)	302	AB	0.5
P(MMA-AA)2	MMA/AA/AIBN = 90/210/10 (by mol.)	11,900 (1.98)	350	—	—
PMVA2	P(MMA-AA)2/AB = 3/1 (by wt.)	14,050 (2.40)	342	AB	0.2
P(MMA-MAn)1	MMA/MAn/AIBN <sup>a</sup> = 90/210/10 (by mol.)	40,770 (1.90)	360	—	—
PMMAAnMA1	P(MMA-MAn)1/HEMA <sup>b</sup> = 3/1 (by wt.)	47,730 (2.32)	250	HEMA	0.5
P(MMA-MAn)2	MMA/MAn/AIBN = 90/210/15 (by mol.)	7,240 (2.05)	380	—	—
PMMAAnMA2	P(MMA-MAn)2/HEMA = 3/1 (by wt.)	8,290 (2.35)	210	HEMA	0.5
P(MMA-MAn)3	MMA/MAn/AIBN = 90/210/15 (by mol.)	9,750 (2.08)	375	—	—
PMMAAnMA3	P(MMA-MAn)3/HEMA = 3/1 (by wt.)	15,690 (2.55)	180	HEMA	0.7

<sup>a</sup>MMA: methyl methacrylate; AA: acrylic acid; MAn: maleic anhydride;<sup>b</sup>AB: allyl bromide; HEMA: hydroxyethyl methacrylate;<sup>c</sup> $M_n$ : number average molecular weight estimated by GPC (eluent: THF; standards: PMMA); and<sup>d</sup>AV = acid value (eq/g).

( $x = 10$  or  $15$ ) in PGMEA;  $[MMA]_0 = 1.1$  M) to attain the prepolymer, denoted as P(MMA-MAn). The acid values (AVs) of the resulting P(MMA-MAn) were approximately 360 and 380 eq/g. Then, we modified the P(MMA-MAn) prepolymers with HEMA (i.e., step svi in Scheme 1c) to produce the abbreviated PMMAAnMA PR system. As shown in Figure 2Aiii,Aiv, the IR spectra of each P(MMA-MAn)1 and PMMAAnMA1 also feature a dominant carbonyl stretching band centered at approximately  $1730\text{ cm}^{-1}$ , indicative of the ester functionality within the polymer structure. Furthermore, distinct C=C double bond stretching vibrations around  $1630\text{ cm}^{-1}$  were obvious in the PMMAAnMA1. As shown in Figure 2Biii,Biv, the corresponding  $^1\text{H}$  NMR spectra reveal well-defined and broadened resonance peaks labeled a''' and b'''. These peaks are attributed to the methylene linkage (approximately 4.2 ppm) and the pendant vinyl groups (approximately 5.4–5.8 ppm) originating from the incorporated HEMA moieties. Collectively, these spectral features validate the successful occurrence of the post-esterification reaction and confirm the presence of vinyl functionalities, thereby supporting the structural integrity and chemical transformation achieved through this synthetic strategy. Table 1 summarizes the reaction conditions and characterization of prepolymers and PRs.

### 3.2 | Compatibility of Photosensitive Resins and BCP Blends

As shown in Table 2, we then composed the first series of PR/BCP blends, containing PMVA1 (having a higher post-esterification fraction), Irgacure 907, and ITX with various PCL-*b*-PnBA weight percentages (i.e., 1%, 5%, 10%, and 30%) in DMAC. The mixtures were coated on glass plates, dried, and peeled to obtain free-standing bulk films with a thickness around  $100\text{ }\mu\text{m}$  and UV-curing reactions were conducted. As shown in Figure 3A, the optical images of all films displayed good transparency, indicating no macrophase separation or agglomeration among the various PMVA1/BCP blends. Subsequently, UV-vis traces in transmittance (%) with a range of 400–700 nm were recorded. As shown in Figure 3B, these bulk films showed similar transmittance in the 60%–70% range. The PMVA1/BCP30wt% sample exhibited a bit lower transmittance than the PMVA1/BCP1% sample. In particular, for the PMVA1/BCP5% sample, a high transmittance with ca. 75% after 550 nm was acquired (i.e., curve b). The small-angle X-ray scattering (SAXS) patterns were further collected to analyze the microstructure information of the UV-cured blend films. As shown in Figure 3C, the SAXS profiles illustrate the corresponding structural evolution of various PMVA1/BCP blends. As the BCP content increases, the scattering peak rises across the measured  $q$ -range, indicating a higher degree of nanoscale structural organization or domain formation. The curves exhibit characteristic broad peaks corresponding to nanostructural periodicities, with  $d$ -spacings ( $d_s$ ) of approximately 33.5 nm for PMVA1/BCP10% and 34.7 nm for PMVA1/BCP30%. As illustrated in Figure S3a, we proposed plausible microphase separation mechanisms via the photo-curing reactions. Referring to Figure S3b and previous reports [59–61], similar solubility parameters ( $\delta$ ) between the PMMA and PCL segments and strong hydrogen bonding between the PAA and PCL segments both positively contributed. It illustrated that the PCL segment acts as a miscible part, whereas the PnBA segment is an excluded part within the PR matrix. With a fast photo-curing reaction, it is rational that a pre-ordered microstructure was initially self-assembled mechanism before crosslinking (i.e., SA mechanism in Figure 3a1). In brief, the SAXS analysis confirms that increasing the BCP concentration enhances nanostructure formation in PMVA1, offering valuable insights for the design of high blending compatibility on a nanoscale with phototunable morphologies. To further examine the development process, the PMVA1 and PMVA1/BCP10% coated copper foil were subjected to UV-irradiation at  $600\text{ mJ/cm}^2$  for 10 min. As shown in Figure S4a,b, the pristine PMVA1 PR showed low development ability when using 1 wt%  $\text{Na}_2\text{CO}_{3(\text{aq})}$  developer and moderate ability when using MeOH developer. Regarding the case of the PMVA1/BCP10% blend, as shown in Figure S4c, the obtained development was much less smooth, and the unexposed

**TABLE 2** | Recipes of the blends of PMAV1, additive, and initiators in weight.

Sample <sup>a</sup>	PMAV1 [g]	PCL- <i>b</i> -PnBA [g]	Irgacure 907 [g]	ITX [g]	DMAc [g]
PMAV1/BCP1% <sup>b</sup>	0.478	0.005	0.012	0.0048	2.82
PMAV1/BCP5%	0.458	0.025	0.0115	0.0046	2.82
PMAV1/BCP10%	0.434	0.05	0.0109	0.0043	2.82
PMAV1/BCP30%	0.338	0.15	0.0085	0.0034	2.82

<sup>a</sup>PMAV1:  $M_n = 20,610$ ; BCP: PCL<sub>119</sub>-*b*-PnBA<sub>96</sub> ( $M_{n,NMR} = 26,080$ ;  $D = 1.28$ ;  $\Phi_{PCL} = 0.49$ ); and

<sup>b</sup>The mixing weight percentage in PMAV1/BCP $x$ % is defined as  $xBCP/(PMAV1 + xBCP) \times 100\%$ .

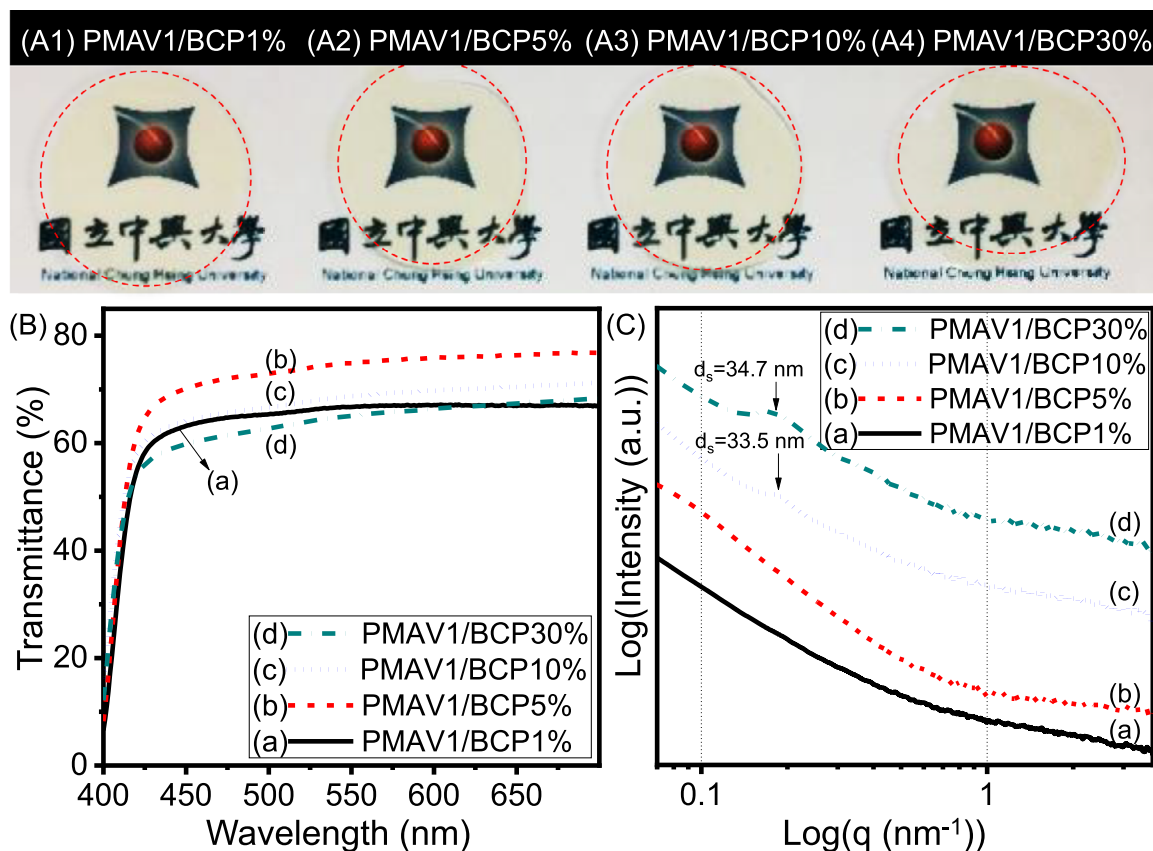


**FIGURE 3** | UV-cured bulk films (thickness = ca. 100  $\mu\text{m}$ ) comprising PMAV1 with various BCP additive weight percentages for compatibility tests of (A) optical images, (B) UV-vis transmittance, and (C) SAXS profiles ( $d_s$  = d-spacing).

area was still covered by the blending film. We speculated that such unsmooth development might take two factors into account: an imbalance in hydrophobic and hydrophilic ratios, and poor solubility with relatively high molecular weight. Accordingly, we then utilized the second PR system of PMMA $n$ MA to fine-tune the PR characteristics.

### 3.3 | Development and Mechanical Reliability Tests of Photosensitive Materials

To maintain the integrity of the membrane surface during pre-testing and ensure that the solvent evaporates, the solvent was replaced with high-boiling solvents such as DMAc, and the pre-baking condition was set to 85°C until the membrane surface was dry enough. As shown in Figure S5a, using a relevant high molec-

ular weight (i.e.,  $M_n$  = ca. 50,000) of PMMA $n$ MA1, the exposure time was 20 min, and the development ability still showed low efficiency. As shown in Figure S5b, using a low molecular weight (i.e.,  $M_n$  = ca. 8,000) of PMMA $n$ MA2, the exposure time was shortened to 1.5 min, and the development performance was significantly improved. This result indicates that the molecular weight affects the developing ability. The photosensitive mixture with moderate molecular weight can be successfully developed within a very short time (1.5 min). After confirming the exposure and development ability of the main resin, it was mixed with additives. The mass-produced PMMA $n$ MA3 was then used for further tests. The morphological stability of PMMA $n$ MA3-based films with and without 30 wt% BCP incorporation was evaluated. Both films remained transparent after development (Figure 4a1,b1), but the BCP-containing film exhibited a smoother and more homogeneous surface, suggesting improved resistance

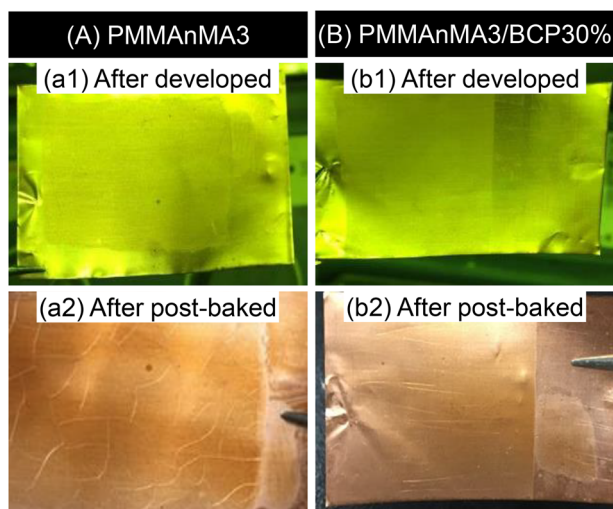


**FIGURE 4** | Development test appearances of (1) after development and (2) after post-baking for the samples of UV-cured (A) PMMAAnMA3 and (B) PMMAAnMA3/BCP30% films (Irgacure 907 (2.5 phr) and ITX (1 phr) mixed in DMAc solvent are used in all samples).

to developer attack and enhanced film uniformity. Upon post-bake treatment (Figure 4a2,b2), the differences became more pronounced. The pristine PMMAAnMA3 film exhibited extensive cracking, reflecting high internal stress and poor thermal tolerance. In contrast, the PMMAAnMA3/BCP30% film preserved its continuity with negligible defects, indicating that the BCP domains effectively dissipated the stress and reinforced thermal robustness. These results demonstrate that the introduction of 30 wt% BCP significantly improves film uniformity, durability, and adhesion.

After confirming the photosensitivity, we examine the physical properties of the samples that are relevant to the practical process. The adhesion and mechanical durability of the PMMAAnMA3-based films were evaluated using cross-cut (100-grid/ASTM D3359 test) and dead-fold tests. In the 100-grid adhesion test (Figure 5a1,b1), both the PMMAAnMA3 and PMMAAnMA3/BCP30% films retained their integrity with minor defects (i.e., 5B level in the 100-grid/ASTM D3359 test), indicating good interfacial adhesion. The dead-fold test method is shown in Figure 5c to further examine the mechanical flexibility. As shown in Figure 5c, for the dead-fold test, the films were subjected to one fore-fold (i.e.,  $180^\circ$  for a half cycle) followed by a back-fold (i.e.,  $360^\circ$  for one cycle). As shown in Figure 5a2,a3,b2–b4, the pristine PMMAAnMA3 film exhibited visible cracks even before deformation, and severe damage appeared after only half a folding cycle, indicating its brittleness under mechanical stress. The PMMAAnMA3/BCP30% film remained intact after curing and withstood three folding cycles with only limited deformation. This superior resistance to cracking indicates that BCP domains effectively dissipate localized stress, improving both toughness and flexibility. The film morphology with circular pattern after exposure and development was assessed by optical microscopy (OM) and scanning electron microscopy (SEM). Pristine PMMAAnMA3 films, analyzed by OM and SEM (Figure 6Sa1,a2), showed poor uniformity and structural robustness due to a rough surface, irregularities, and fractured domains. In contrast, the PMMAAnMA3/BCP30% film (Figure 6Sb1,b2) was

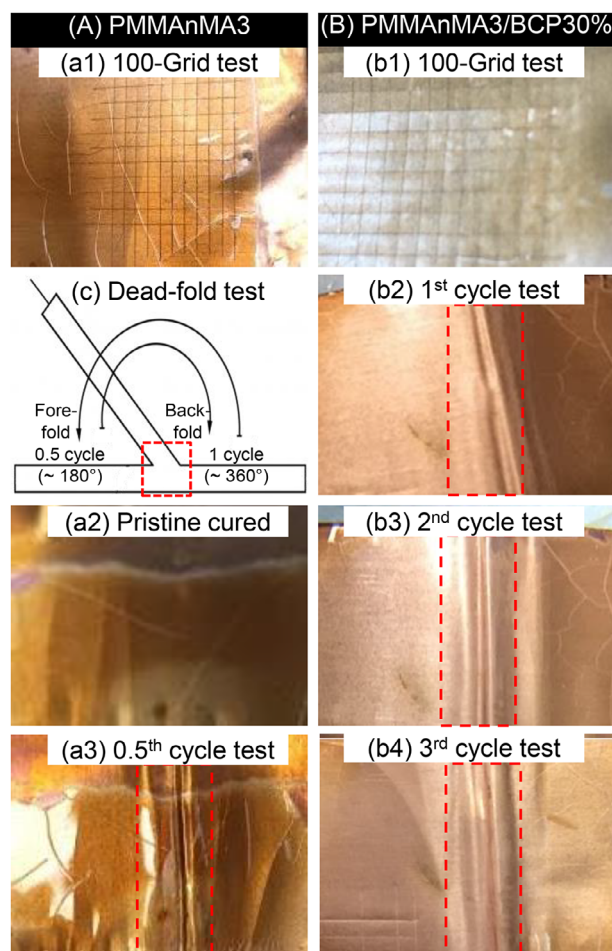


**FIGURE 5** | Mechanical reliability evaluations via (1) 100-grid test (ASTM D3359) and (c, 2–4) dead-fold cycle tests of PMMAAnMA3 and PMMAAnMA3/BCP30% films (all recipes have Irgacure 907 (2.5 phr) and ITX (1 phr) and mixed in DMAc solvent; red-dashed areas indicate the bending areas).

smoother and more homogeneous in a resolution scale of about  $200\ \mu\text{m}$ , displaying regular, circular domains with fewer cracks, indicating improved stability and toughness. These results confirm that while neat PMMAAnMA3 lacks mechanical reliability, incorporation of 30 wt% BCP significantly enhances adhesion, fold endurance, and morphological quality, underscoring its potential in robust photoresist and coating applications. Figure S7 shows the SAXS profiles of PMMAAnMA3 blended with different BCP contents. The PMMAAnMA/BCP5% film (i.e., Figure S7a) showed only weak, broad scattering in a sphere morphology (SPH) without a clear secondary scattering peak, reflecting less-ordered phase separation at low BCP concentration with a characteristic  $d_s$  of ca.  $41\ \text{nm}$ . The PMMAAnMA3/BCP30% sample (Figure S7b) exhibited distinct scattering peaks with a clear secondary scattering peak, corresponding to a characteristic  $d_s$  of ca.  $31\ \text{nm}$  in a highly ordered lamellae morphology (LAM). TEM analysis of the PMMAAnMA3/BCP blends containing 5% and 30% BCP showed distinct differences in morphology. At 30% BCP, a well-defined lamellar structure was observed. In contrast, the 5% BCP sample exhibited no discernible microphase-separated morphology, which is likely due to the insufficient concentration of BCP (Figure S9).



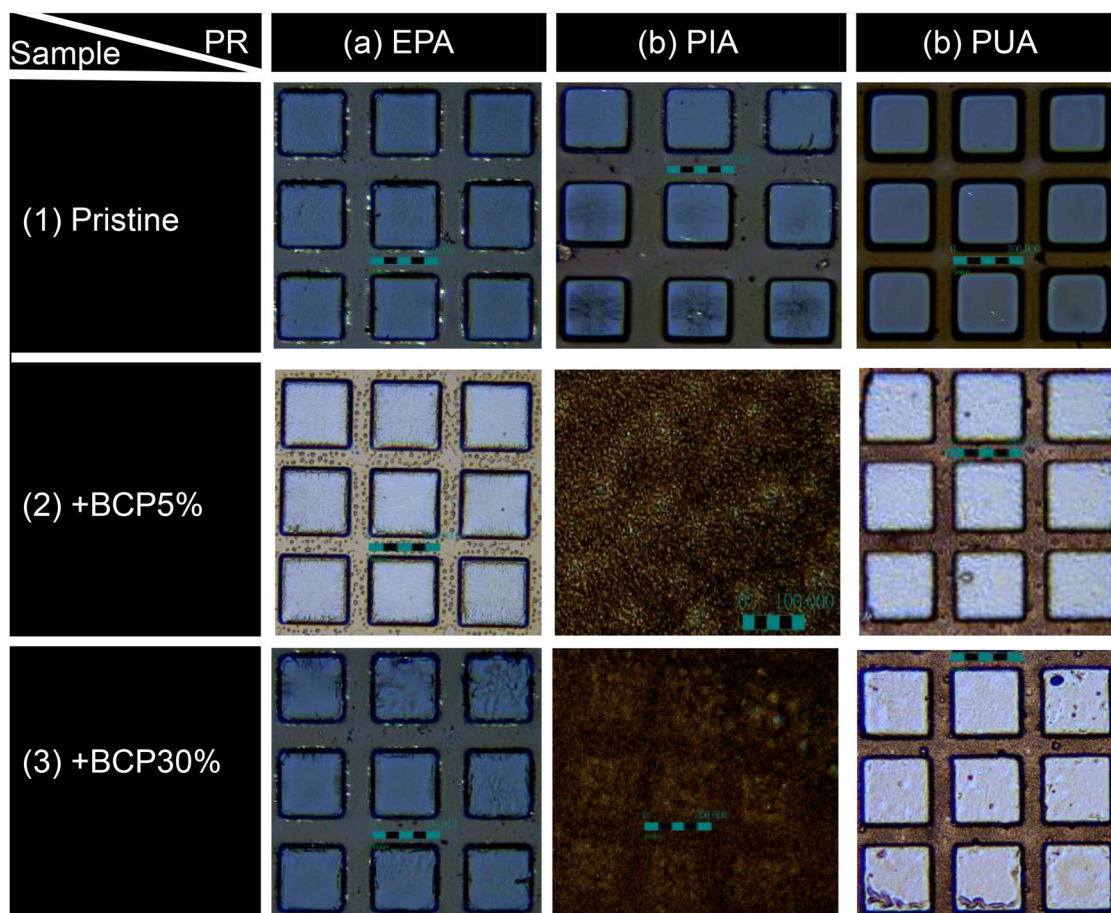


**FIGURE 6** | OM images for the development of various formulations of commercial PRs: (a) epoxy acrylate (EPA), (b) polyimide acrylate (PIA), and (c) polyurethane acrylate (PUA)—containing PCL-b-PnBA BCP additives at different weight loadings: (1) pristine, (2) +5%, and (3) +30% (bar = 200  $\mu\text{m}$ ).

### 3.4 | Development and Mechanical Reliability Tests of Photosensitive Materials

We then formulated commercial PRs, including epoxy acrylate (EPA), polyimide acrylate (PIA), and polyurethane acrylate (PUA), that inherently possess good film-forming properties as shown in Figure S8a1–c1. After the incorporation of the BCP additive (Figure S8a2–c3, the films retained their inherent film-forming capability and achieved enhanced miscibility and improved morphological uniformity. This indicates that BCP acts as a compatibilizer and stabilizer rather than merely providing continuity to the film. Therefore, the observed improvements represent a synergistic effect between the intrinsic film-forming nature of commercial PRs and the microphase-stabilizing role of BCP. The imaging performance of the three commercial PR systems (EPA, PIA, and PUA) showed notable differences after further exposure and development. Figure 6a1–a3, c1–c3 show that both EPA and PUA formulations maintained good pattern fidelity with clear square features and sharp edges (scale bar = 200  $\mu\text{m}$ ), even after blending with different amounts of BCP. These results indicate that the inherent film-forming ability of EPA and PUA, combined with the compatibilizing role of BCP, ensures stable morphology and reliable imaging quality. In contrast, the PIA-based formulation (Figure 6b2,b3) exhibited poor image quality, with patterns becoming indistinct and severely degraded upon development. The loss of feature integrity illustrates that PIA

suffers from insufficient resistance to developer treatment and weak structural stability, which cannot be compensated for by BCP addition.

Compatibility and nanoscale organization studies were examined on the UV-cured bulk films prepared using commercial EPA and PUA PRs with 5 and 30 wt% additives. As shown in Figure 7a1,b2, all samples displayed transparent and uniform films without visible phase separation or macroscopic defects, indicating the occurrences of the SA mechanism within the EPA and PUA matrix. The SAXS profiles revealed well-defined scattering peaks corresponding to spacings of ca. 52 nm for the EPA blends (i.e., curves Figure 7c1,c2) and ca. 33 nm for the PUA blends (i.e., curves Figure 7d1,d2). The inserted cartoon figures illustrate our proposed relevant microstructures. Notably, the presence of significant scattering features at a higher BCP loading in the case of EPA/BCP30% film reveals enhanced long-range ordering compared with lower concentrations. The dead-fold cycle test results of commercial PRs blended with additives on copper foil are summarized in Table S2. The data clearly indicate 2–3-fold increases in durability in the dead-fold tests upon the incorporation of the BCP additive. In brief, the results of optical homogeneity, nanoscale SAXS profiles, and enhanced dead-fold durability strongly support the conclusion that the BCP can also be applied to EPA and PUA PRs with excellent compatibility and contained microphase separation inside.

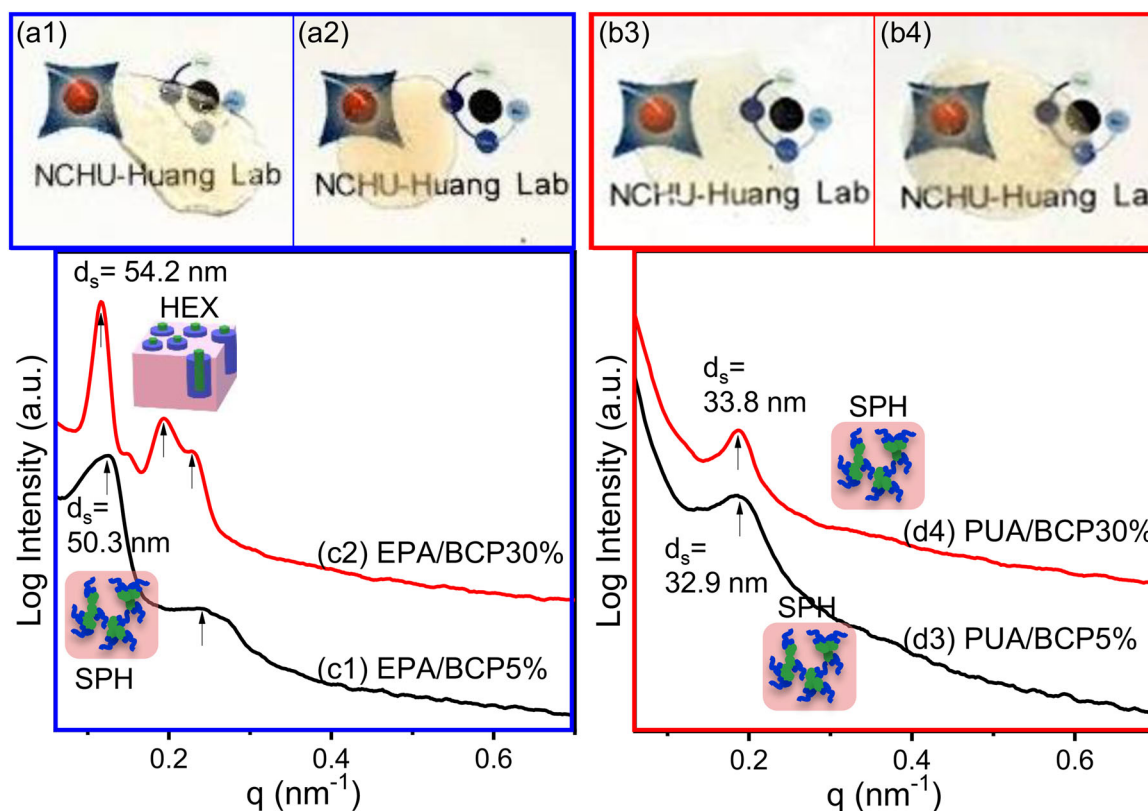


**FIGURE 7** | UV-cured bulk films (thickness = ca. 100  $\mu\text{m}$ ) of (a, b) optical images and (c, d) SAXS profiles: (1) EPA/BCP5%, (2) EPA/BCP30%, (3) PUA/BCP5%, and (4) PUA/BCP30% ( $d_s$  = d-spacing; HEX = hexagonal cylinder; SPH = sphere).

#### 4 | Conclusions

This study demonstrated the successful synthesis of PCL-*b*-PnBA BCPs through an efficient combination of ROP-*C*-SARA ATRP approach, using the dual-functional initiator HEBiB. Characterization by  $^1\text{H}$  NMR and GPC confirmed the high purity and well-defined structure of the obtained BCPs, showing moderate molecular weight ( $M_{n,\text{NMR}} = 26\,080$ ) and narrow dispersity values ( $\bar{D} < 1.3$ ), indicative of controlled/living polymerization behavior.

The synthesized PCL-*b*-PnBA BCP was incorporated into two photoresist (PR) systems. Initial compatibility tests with PMAVI revealed high transparency and nanoscale structural organization driven by the SA mechanism. Further optimization using the PMMA3 system showed that adding 30 wt% of BCP significantly improved film properties. The resulting PMMA3/BCP30% films exhibited excellent adhesion, flexibility, and toughness, withstanding multiple dead-fold cycles due to effective stress dissipation via well-ordered lamellar BCP domains.

In addition, the BCP additive proved effective in commercial PRs, including EPA and PUA. The UV-cured films remained transparent and uniform, confirming successful microphase formation. SAXS analysis revealed distinct scattering peaks with characteristic domain spacings of approximately 52 nm (EPA) and 33 nm (PUA). Dead-fold tests further showed a 2–3-fold enhancement in durability, while maintaining the film-forming quality

and compatibility of the base resins. These results highlight the strong potential of PCL-*b*-PnBA as a versatile additive to improve mechanical reliability and performance in advanced photoresist systems.

#### Author Contributions

M.-F.H. and C.-F.H. designed the experiments and contributed to the funding acquisition; S.Y.E., T.B., H.-M.W., and K.-Y. K. conducted the experiments, measurements, and data analysis; S.Y.E., T.B., and S.-W.K. analyzed the data and wrote the relevant contents. S.Y.E. and T.B. wrote the original draft; M.-F.H. and C.-F.H. summarized and edited all the contents.

#### Acknowledgements

The NCHU authors would like to thank Zhen Ding Technology Holding Limited and the National Science and Technology Council (NSTC114-2811-E-005-003) for funding. T.B., C.-F.H., and S.-W.K. acknowledge TCUS joint support. The National Synchrotron Radiation Research Center (NSRRC), Taiwan, was deeply acknowledged for SAXS experiments.

#### Conflicts of Interest

The authors declare no conflicts of interest.

#### Data Availability Statement

The data that support the findings of this study are available from the corresponding author upon reasonable request.



## References

1. M. Hassaan, U. Saleem, A. Singh, A. J. Haque, and K. Wang, "Recent Advances in Positive Photoresists: Mechanisms and Fabrication," *Materials* 17 (2024): 2552, <https://doi.org/10.3390/ma17112552>.
2. C. Luo, C. Xu, L. Lv, H. Li, X. Huang, and W. Liu, "Review of Recent Advances in Inorganic Photoresists," *RSC Advances* 10 (2020): 8385–8395.
3. L. Schittecatte, V. Geertsens, D. Bonamy, T. Nguyen, and P. Guenoun, "From Resin Formulation and Process Parameters to the Final Mechanical Properties of 3D Printed Acrylate Materials," *MRS Communication* 13 (2023): 357–377.
4. B. Du, X. Zhou, Q. Liet al., "Surface Treat Method to Improve the Adhesion Between Stainless Steel and Resin: A Review," *ACS Omega* 8 (2023): 39984, <https://doi.org/10.1021/acsomega.3c05728>.
5. J. Liu, D. Wang, Y. Liet al., "Exceptional Lithography Sensitivity Boosted by Hexafluoroisopropanols in Photoresists," *Polymers* 16 (2024): 825, <https://doi.org/10.3390/polym16060825>.
6. J. Gao, S. Zhang, X. Cui, et al., "Optimization Strategy for Epoxy Cross-Linked Molecular Glass Photoresist in EUV Lithography," *Journal of Photochemistry and Photobiology A: Chemistry* 453 (2024): 115684, <https://doi.org/10.1016/j.jphotochem.2024.115684>.
7. J. Liu, X. Zheng, H. Li, R. Liu, Q. Mu, and X. Liu, "Synthesis of Novel Branched UV-Curable Methacrylate Copolymer and Its Application in Negative Photoresist," *Polymer Bulletin* 72 (2015): 523–533, <https://doi.org/10.1007/s00289-014-1289-9>.
8. Y. Zheng, X. Xin, Q. Yang, Z. Zhang, Z. Zhou, and Y. Ma, "Exploring the Development of Photoresists in Lacquer Under the Background of Global Carbon Neutrality: A Mini Review," *Coatings* 14 (2024): 994, <https://doi.org/10.3390/coatings14080994>.
9. J. Liu and W. Kang, "New Chemically Amplified Positive Photoresist With Phenolic Resin Modified by GMA and BOC Protection," *Polymers* 15 (2023): 1598, <https://doi.org/10.3390/polym15071598>.
10. A. Al Rashid, W. Ahmed, M. Y. Khalid, and M. Koç, "Vat Photopolymerization of Polymers and Polymer Composites: Processes and Applications," *Additive Manufacturing* 47 (2021): 102279.
11. S. Zhang, L. Chen, J. Gao, et al., "Chemically Amplified Molecular Glass Photoresist Regulated by 2-Aminoanthracene Additive for Electron Beam Lithography and Extreme Ultraviolet Lithography," *ACS Omega* 8 (2023): 26739.
12. V. Vlnieska, A. Mikhaylov, M. Zakharova, E. Blasco, and D. Kunka, "Epoxy Resins for Negative Tone Photoresists," *Polymers* 11 (2019): 1457, <https://doi.org/10.3390/polym11091457>.
13. Y. Ding, Y. Xin, Q. Zhang, and Y. Zou, "Acrylic resins with Oxetane Pendant Groups for Free Radical and Cationic Dual-Curing Photoresists," *Materials & Design* 213 (2022): 110370, <https://doi.org/10.1016/j.matdes.2021.110370>.
14. X. Sun, K. Hu, K. Wang, C. Su, R. Wang, and Z. Ma, "Hydrophilic Surface Modification of Poly(methyl methacrylate)/Poly(methyl methacrylate-co-acrylic acid) Composite Film by Surface Activation," *Macromolecular Chemistry and Physics* 225 (2024): 2300312, <https://doi.org/10.1002/macp.202300312>.
15. Z. Zhang, P. Niu, Z. Zhao, et al., "Co-Enhancement of Toughness and Strength of Room-Temperature Curing Epoxy Adhesive Derived from Hydroxyl-Terminated Polybutadiene-Based Polyurethane Resin," *European Polymer Journal* 219 (2024): 113373, <https://doi.org/10.1016/j.eurpolymj.2024.113373>.
16. R. Han, X. Ma, L. Cai, Z. Zhang, Y. Fang, and J. Wang, "Low Viscosity and Low Temperature Curing Reactive Poss/Epoxy Hybrid Resin with Enhanced Toughness and Comprehensive Thermal Performance," *RSC Advances* 14 (2024): 7263–7275.
17. C. Zhang, J. Cui, W. Sui, et al., "High Heat Resistance, Strength, and Toughness of Epoxy Resin with Cellulose Nanofibers and Structurally Designed Ionic Liquid," *Chemical Engineering Journal* 478 (2023): 147063, <https://doi.org/10.1016/j.cej.2023.147063>.
18. Y. Xi, H. Fukuzawa, G. Kikugawa, et al., "Enhancing Epoxy Resin Curing: Investigating the Catalytic Role of Water as a Trace Impurity in Dense Crosslinked Network Formation Using an Advanced cat-GRRM/MC/MD Method1," *Polymer* 313 (2024): 127675, <https://doi.org/10.1016/j.polymer.2024.127675>.
19. J. Fan and A. Chen, "Studying a Flexible Polyurethane Elastomer With Improved Impact-Resistant Performance," *Polymers* 11 (2019): 467, <https://doi.org/10.3390/polym11030467>.
20. L. Shuilan, W. Shuanjin, H. Sheng, et al., "Super Anti-Water Permeability and High Toughness of CO<sub>2</sub>-Derived Polycarbonate Polyurethane via Copolymerization with Polydimethylsiloxane," *Macromolecular Chemistry and Physics* 226 (2025): 202500139.
21. J. Zhang, J. Tian, T. Wang, et al., "High-Reliable Polyurethane Modified Epoxy Photosensitive Composites for Solder Resist Applications," *Composites Communications* 53 (2025): 102180, <https://doi.org/10.1016/j.coco.2024.102180>.
22. M. Ito, H. Takamatsu, T. Taniguchi, H. Okamoto, and T. Karatsu, "Effect of Acrylic and Epoxy Hybrid Crosslinker on the Mechanical Strength of Photocurable Resin for 3D Printing," *Journal of Photopolymer Science and Technology* 34 (2021): 237–249, <https://doi.org/10.2494/jphotopolymer.34.237>.
23. Q. Lin, W. Zhang, L. Chen, et al., "Rigid Photosensitive Polyimide Significantly Improves the Comprehensive Performance of UV-Curing Epoxy Acrylic Resins," *ACS Applied Polymer Materials* 6 (2024): 8267–8276, <https://doi.org/10.1021/acsapm.4c01133>.
24. L. Feng, R. Li, H. Yang, S. Chen, and W. Yang, "The Hyperbranched Polyester Reinforced Unsaturated Polyester Resin," *Polymers* 14 (2022): 1127, <https://doi.org/10.3390/polym14061127>.
25. E. Serrano, A. Tercjak, C. Ocando, et al., "Curing Behavior and Final Properties of Nanostructured Thermosetting Systems Modified With Epoxidized Styrene-Butadiene Linear Diblock Copolymers," *Macromolecular Chemistry and Physics* 208 (2007): 2281–2292, <https://doi.org/10.1002/macp.200700169>.
26. C. Wu, F. Xu, H. Wang, H. Liu, F. Yan, and C. Ma, "Manufacturing Technologies of Polymer Composites—A Review," *Polymers* 15 (2023): 712, <https://doi.org/10.3390/polym15030712>.
27. M. Bilugali Mahadevaswamy, R. Aradhya, S. Bhattacharya, and S. R. Jagannathan, "Effect of hybrid carbon nanofillers at percolation on electrical and mechanical properties of glass fiber reinforced epoxy," *Journal of Applied Polymer Science* 139 (2022): 52439, <https://doi.org/10.1002/app.52439>.
28. J. A. Campbell, H. Inglis, E. Ng WeiLong, C. McKinley, and D. A. Lewis, "Morphology Control in a Dual-Cure System for Potential Applications in Additive Manufacturing," *Polymers* 11 (2019): 420, <https://doi.org/10.3390/polym11030420>.
29. Y. Li, L. Yang, H. He, et al., "In Situ Photodeposition of Platinum Clusters on a Covalent Organic Framework for Photocatalytic Hydrogen Production," *Nature Communications* 13 (2022): 1355, <https://doi.org/10.1038/s41467-022-29076-z>.
30. G. Sun, X. Wu, and R. Liu, "A Comprehensive Investigation of Acrylates Photopolymerization Shrinkage Stress from Micro and Macro Perspectives by Real Time MIR-Photo-Rheology," *Progress in Organic Coatings* 155 (2021): 106229, <https://doi.org/10.1016/j.porgcoat.2021.106229>.
31. M. Topa-Skwarczyńska and J. Ortyl, "Photopolymerization Shrinkage: Strategies for Reduction, Measurement Methods and Future Insights," *Polymer Chemistry* 14 (2023): 2145–2158, <https://doi.org/10.1039/D3PY00261F>.
32. Z. Yang, J. Shan, Y. Huang, et al., "Preparation and Mechanism of Free-Radical/Cationic Hybrid Photosensitive Resin with High Tensile Strength for Three-Dimensional Printing Applications," *Journal of Applied Polymer Science* 138 (2021): 49881, <https://doi.org/10.1002/app.49881>.

33. L. Ning, J. Chen, J. Sun, Y. Liu, D. Yi, and J. Cao, "Preparation and Properties of 3D Printing Light-Curable Resin Modified With Hyperbranched Polysiloxane," *ACS Omega* 6 (2021): 23683–23690, <https://doi.org/10.1021/acsomega.1c01232>.
34. M. Topa-Skwarczyńska, W. Wańczyk, F. Petko, et al., "Increasing Resolution in Additive Manufacturing by Using High-Performance and Non-Toxic Photoinitiating Systems," *Additive Manufacturing* 94 (2024): 104473.
35. T. Wang, C. Zhuang, G. Yang, H. Xin, L. Jiang, and J. Zhang, "Interface Engineering of Underlayer of Chemically-Amplified EUV Photoresists to Enhance the Photolithographic Performance," *Materials Science and Engineering: B* 307 (2024): 117539, <https://doi.org/10.1016/j.mseb.2024.117539>.
36. M. Hanzawa, T. Ogura, M. Akamatsu, K. Sakai, and H. Sakai, "Enhanced Removal of Photoresist Films Through Swelling and Dewetting Using Pluronic Surfactants," *Langmuir* 39 (2023): 14670–14679, <https://doi.org/10.1021/acs.langmuir.3c02034>.
37. M. W. Hasan, L. Deeb, S. Kumanaiev, C. Wei, and K. Wang, "Recent Advances in Metal-Oxide-Based Photoresists for EUV Lithography," *Micromachines* 15 (2024): 1122, <https://doi.org/10.3390/mi15091122>.
38. S. Penczek and J. Pretula, "Activated Monomer Mechanism (AMM) in Cationic Ring-Opening Polymerization. The Origin of the AMM and Further Development in Polymerization of Cyclic Esters," *ACS Macro Letters* 10 (2021): 1377–1397, <https://doi.org/10.1021/acsmacrolett.1c00509>.
39. M. Szewczyk-Lagodzińska, A. Plichta, M. Dębowski, S. Kowalczyk, A. Iuliano, and Z. Florjańczyk, "Recent Advances in the Application of ATRP in the Synthesis of Drug Delivery Systems," *Polymers* 15 (2023): 1234, <https://doi.org/10.3390/polym15051234>.
40. Y.-S. Huang, J.-K. Chen, T. Chen, and C.-F. Huang, "Synthesis of PNVP-Based Copolymers with Tunable Thermosensitivity by Sequential Reversible Addition–Fragmentation Chain Transfer Copolymerization and Ring-Opening Polymerization," *Polymers* 9 (2017): 231, <https://doi.org/10.3390/polym9060231>.
41. K.-Y. Lai, Y.-S. Huang, C.-Y. Chu, and C.-F. Huang, "Synthesis of Poly(N-H benzamide)-b-poly(lauryl methacrylate)-b-poly(N-H benzamide) Symmetrical Triblock Copolymers by Combinations of CGCP, SARA ATRP, and SA ATRC," *Polymer* 137 (2018): 385–394, <https://doi.org/10.1016/j.polymer.2018.01.033>.
42. Y.-S. Huang, D. D. Ejeta, S.-W. Kuo, Y. Nakamura, and C.-F. Huang, "Combinations (  $\epsilon$  ) Among Controlled/Living Polymerizations and Utilizations of Efficient Chemical Reactions for the Synthesis of Novel Polymeric Materials," *Polymer Chemistry* 14 (2023): 4783–4803, <https://doi.org/10.1039/D3PY00997A>.
43. M. Göktaş and Ü. Aslan, "Synthesis and Characterization of Graft Copolymer Hydrogel by "Grafting From" Atom Transfer Radical Polymerization Using Brominated Macro Monomeric Initiator and Investigation of Hydrogel Properties," *Polymer Bulletin* 81 (2024): 11127–11143.
44. C. Aydoğan, C. Kutahya, A. Allushi, G. Yilmaz, and Y. Yagci, "Block Copolymer Synthesis in One Shot: Concurrent Metal-Free ATRP and ROP Processes Under Sunlight," *Polymer Chemistry* 8 (2017): 2899–2903, <https://doi.org/10.1039/C7PY00069C>.
45. W. Gao, Y. Guo, J. Cui, et al., "Dual-Curing Polymer Systems for Photo-Curing 3D Printing," *Additive Manufacturing* 85 (2024): 104142.
46. J. Li, L. Chun, Z. Zhang, X. Zhou, and J. Nie, "Block Copolymer Synthesis and Photoinitiated Grafting via a Dual-Wavelength Photoinitiating System Based on Iragcure 2959 Derivative/Camphorquinone," *European Polymer Journal* 234 (2025): 114022, <https://doi.org/10.1016/j.eurpolymj.2025.114022>.
47. D. T. Meiers, M. Rothhammer, M. Maier, C. Zollfrank, and G. von Freymann, "Utilizing the Sensitization Effect for Direct Laser Writing in a Novel Photoresist Based on the Chitin Monomer N-acetyl-D-glucosamine," *Advanced Engineering Materials* 25 (2023): 2201688, <https://doi.org/10.1002/adem.202201688>.
48. C.-F. Huang, W.-H. Chen, J. Aimi, et al., "Synthesis of Well-Defined PCL- b -PnBA- b -PMMA ABC-type Triblock Copolymers: Toward the Construction of Nanostructures in Epoxy Thermosets," *Polymer Chemistry* 9 (2018): 5644–5654, <https://doi.org/10.1039/C8PY01357H>.
49. Y.-S. Huang and C.-F. Huang, "Synthesis of Well-Defined PMMA-b-PDMS-b-PMMA Triblock Copolymer and Study of Its Self-Assembly Behaviors in Epoxy Resin," *European Polymer Journal* 160 (2021): 110787, <https://doi.org/10.1016/j.eurpolymj.2021.110787>.
50. M. Michelas, N. Corrigan, and C. Boyer, "3D Printing via Polymerization-Induced Microphase Separation Using Acrylate Macromonomers Instead of macroRAFT Agents," *Polymer Chemistry* 16 (2025): 4102–4112, <https://doi.org/10.1039/d5py00226e>.
51. S. Maekawa, T. Seshimo, T. Dazai, et al., "Chemically Tailored Block Copolymers for Highly Reliable sub-10-nm Patterns by Directed Self-Assembly," *Nature Communications* 15 (2024): 5671, <https://doi.org/10.1038/s41467-024-49839-0>.
52. K. Lee, N. Corrigan, and C. Boyer, "Polymerization Induced Microphase Separation for the Fabrication of Nanostructured Materials," *Angewandte Chemie International Edition* 62 (2023): 202307329.
53. R. Kalinova, K. Mladenova, S. Petrova, J. Dumanov, and I. Dimitrov, "Solvent-Free Synthesis of Multifunctional Block Copolymer and Formation of DNA and Drug Nanocarriers," *Nanomaterials* 13 (2023): 2936, <https://doi.org/10.3390/nano13222936>.
54. G. Ö. Kayan and A. Kayan, "Polycaprolactone Composites/Blends and Their Applications Especially in Water Treatment," *ChemEngineering* 7 (2023): 104, <https://doi.org/10.3390/chemengineering7060104>.
55. B. Meng, J. Deng, Q. Liu, Z. Wu, and W. Yang, "Transparent and Ductile Poly(lactic acid)/poly(butyl acrylate) (PBA) Blends: Structure and Properties," *European Polymer Journal* 48 (2012): 127–135, <https://doi.org/10.1016/j.eurpolymj.2011.10.009>.
56. A. Sharma, D. Agarwal, and J. Singh, "Study of Curing Kinetics and Thermal Degradation of UV Curable Epoxy Acrylate Resin," *Journal of Chemistry* 5 (2008): 904–913, <https://doi.org/10.1155/2008/697371>.
57. D. A. Corbin and G. M. Miyake, "Photoinduced Organocatalyzed Atom Transfer Radical Polymerization (O-ATRP): Precision Polymer Synthesis Using Organic Photoredox Catalysis," *Chemical Reviews* 122 (2022): 1830–1874, <https://doi.org/10.1021/acs.chemrev.1c00603>.
58. J. Lyu, Y. Miao, Z. Li, et al., "Where is the Induction From? Effect of Disproportionation and Comproportionation in Cu(0)-mediated Reversible Deactivation Radical Polymerization," *Polymer* 280 (2023): 126055, <https://doi.org/10.1016/j.polymer.2023.126055>.
59. C.-F. Huang and F.-C. Chang, "Comparison of Hydrogen Bonding Interaction Between PMMA/PMAA Blends and PMMA-co-PMAA Copolymers," *Polymer* 44 (2003): 2965–2974, [https://doi.org/10.1016/S0032-3861\(03\)00188-5](https://doi.org/10.1016/S0032-3861(03)00188-5).
60. C.-F. Huang, H.-F. Lee, S.-W. Kuo, H. Xu, and F.-C. Chang, "Star Polymers via Atom Transfer Radical Polymerization From Adamantane-Based Cores," *Polymer* 45 (2004): 2261, <https://doi.org/10.1016/j.polymer.2004.01.051>.
61. C.-F. Huang, S.-W. Kuo, H.-C. Lin, et al., "Thermal Properties, Miscibility and Specific Interactions in Comparison of Linear and Star Poly(methyl methacrylate) Blend with Phenolic," *Polymer* 45 (2004): 5913–5921, <https://doi.org/10.1016/j.polymer.2004.05.043>.

## Supporting Information

Additional supporting information can be found online in the Supporting Information section.

**Supporting File:** macp70153-sup-0001-SuppMat.docx.